Applied Physics B (2022) 128:30
https://doi.org/10.1007/s00340-022-07757-3

Applied Physics B
Lasers and Optics

Wavelength-scanned all-fiber cavity ring-down gas sensing using an L-band active fiber loop

Mengpeng Hu[1,2] · Mai Hu[1] · Weibiao Wang[1] · Qiang Wang[1,2]

Received: 15 November 2021 / Accepted: 10 January 2022 / Published online: 25 January 2022

Abstract
We report an all-fiber wavelength-scanned cavity ring-down technique using an L-band active fiber loop. A software-based wavelength scanning scheme is developed to automatically sweep the absorption line of the analyte, by which the empty cavity loss can be directly obtained as well as the absorption information. Hence, analyte information can be further quantified by analyzing the whole calibration-free absorption spectrum. We choose the absorption transition of $R(14)$ of CO_2, as an example, for demonstration. The recovered absorption spectrum matches the theoretically computed absorption profile well with an R^2 value of 0.9964. Under an optimized integration time of 308 s, the sensing system shows a noise equivalent absorption coefficient of 2.15×10^{-6} cm^{-1}, suggesting its potential applications to gas sensing with easy optical assembly, simple operation, and long-term stability.

1 Introduction

Cavity ring-down spectroscopy (CRDS) is a well-established technique for detecting and quantifying gas species. In the CRDS, a pair of mirrors with high reflectivity enables the significant extension of laser-gas interaction length in a restricted geometric space [1–4]. Instead of measuring the attenuation of transmitted light through the target gas, CRDS measures the intensity decay rate of light pulses inside a high-finesse optical cavity, contributing to the unique low susceptibility to laser noise. It also inherits the merits of traditional direct absorption spectroscopy, such as high selectivity and fast response. Besides, the near-infrared (NIR) absorption spectroscopy for gas analysis has attracted much attention due to the advantages of mature fiber optics, such as the intrinsic safety in hazardous conditions, availability of low-cost components, and the capability of multiplexing [5]. Meanwhile, many pollutants and inflammable gases, such as CO_2, HCN, H_2S, C_2H_2, and NH_3, have absorption lines in this region [6].

To date, numerous studies focus on advancing CRDS by performing NIR detection with all-fiber configuration, i.e., fiber loop ring-down spectroscopy (FLRDS) since the proof of concept in 2001 [7] and the pioneering gas sensing demonstration in 2003 [8]. Active fiber loops, as the gain medium, are then adopted to compensate excessive losses in the cavity and to extend the ring down trips to hundreds of microseconds [7, 9–13]. The utilization of fiber loops avoids many complications of the free-space regime, e.g., challenging mode matching and beam quality limitation [5, 14, 15]. Thus, the fiber loop-assisted CRDS system could be made with high flexibility, low cost, and highly robust, allowing a better field application prospect for gas sensing.

Usually, the background of CRDS without absorption, i.e., empty cavity loss, has to be carefully calibrated to identify the absorption-induced cavity loss. Whereas, in practical applications, the inherent background could vary due to the slow and inevitable fluctuation of temperature or strain [12, 16]. Potential errors could be introduced into gas concentration retrieval if the non-absorption cavity loss fluctuation cannot be accurately quantified. Some typical studies have been carried out to suppress this issue by frequent background recalibration. Y. Zhao et al. reported a dual-wavelength differential absorption method, in which two distributed feedback laser diodes (DFB-LDs) with different wavelengths are employed. The system stability was improved by differencing the sensing signal and the background, nevertheless, at the expense of system complexity

✉ Qiang Wang
wangqiang@ciomp.ac.cn

[1] State Key Laboratory of Applied Optics, Changchun Institute of Optics, Fine Mechanics and Physics, Chinese Academy of Sciences, Changchun 130033, China

[2] University of Chinese Academy of Sciences, Beijing 100049, China

and cost [16]. Alternatively, C. Zhu et al. improved this idea by applying square wave modulation to the same DFB-LD. The periodical high and low driving currents generate the two different wavelengths [12]. However, the wavelength shifts of diode lasers during long-term operation[17, 18] remain unsolved if only a dual-wavelength regime is employed, which would further cause systematic errors for gas sensing, especially in a harsh operation condition.

In this paper, we demonstrate a simpler gas sensing technique by combining an active L-band fiber loop and a tunable FLRDS method. A wavelength scanning process is developed, which can simultaneously obtain the cavity background and recover the whole absorption spectrum within the same sweep. Thus, the slow fluctuation of the inherent cavity loss and the drift of the laser frequency can be automatically compensated. To achieve a stable ring down during wavelength scanning, the operation wavelength of the active fiber loop is locked to the seed laser using a fiber Bragg grating-assisted (FBG) filter. Its feasibility is demonstrated by the detection of CO_2 and its concentration is retrieved from the integral absorption area, showing a good match to the theoretical computation using the HITRAN database. This study provides a simple way to improve the long-term system stability of FLRDS gas sensing.

2 Fundamentals of wavelength-scanned FLRDS

With a narrow pulse light injected into the fiber loop, a decaying pulse train will be coupled out in equal intervals as the laser pulse rings down inside the fiber cavity. The intensity of the light after one cavity round trip is $I_0 e^{-\delta/4.343}$, where I_0 is the initial intensity, δ is the round-trip loss of the fiber loop [16]. After m round-trips, the pulse decays are expressed as [5, 16],

$$I_m = I_0 e^{-m\delta/4.343} = I_0 e^{-\delta t/4.343\tau}, \tag{1}$$

where t represents the time taken for m round-trips, τ is the round-trip time. Then, the 1/e ring-down time t_r can be written as [7].

$$t_r = \frac{4.343\tau}{\delta}. \tag{2}$$

Considering the gain of the active fiber and gas absorption, the total round-trip loss δ with the presence of target gas can be expressed as

$$\delta = \delta_0 - G_{\mathrm{EDFA}} + \delta_{\mathrm{gas}}(\nu), \tag{3}$$

where δ_0 is the inherent cavity loss, G_{EDFA} is the gain of EDFA, and $\delta_{\mathrm{gas}}(\nu)$ is gas absorption-induced cavity loss. Ideally, high sensitivity can be achieved by extending the ring-down time when the active loop is running close to a threshold, i.e., $\delta_0 - G_{\mathrm{EDFA}} = 0$. However, a tradeoff between the sensitivity and system stability must be considered, as gain fluctuations of EDFA could be observed at the threshold condition [9, 19]. Combing the Beer–Lambert law, $\delta_{\mathrm{gas}}(\nu)$ profile with optical frequency ν can be written as [16, 20]:

$$\delta_{\mathrm{gas}}(\nu) = -\ln\left(I/I_0\right) = 4.343 \cdot S(T) g(\nu) PCL, \tag{4}$$

$$A = \int \frac{\delta_{\mathrm{gas}}(\nu)}{4.343} \mathrm{d}\nu = S(T)PCL, \tag{5}$$

where $S(T)$ is the molecular absorption linestrength, $g(\nu)$ is the normalized lineshape function, P is the total pressure of the gas cell, C is the target gas concentration, L is the optical path length through the absorbing gas, and A is the integral area of absorption profile. Thus, the gas concentration can be obtained as:

$$C = \frac{A}{S(T)PL} = \frac{\int \delta_{gas}(\nu)\mathrm{d}\nu}{4.343 \cdot S(T)PL} \tag{6}$$

Given that $S(T)$, P and L can be easily known or calibrated in advance for one specific sensor, therefore, to retrieve the target gas concentration, one only needs to acquire the absorption corresponded $\delta_{\mathrm{gas}}(\nu)$ shape using Eq. (3), in which the total cavity loss δ and the non-absorption background, i.e., $\delta_0 - G_{\mathrm{EDFA}}$, can be directly measured within one sweep by simply scanning the laser frequency ν (shown in Fig. 1).

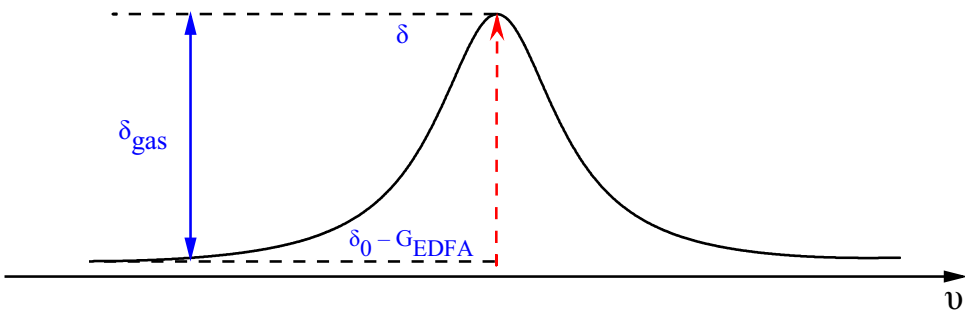

Fig. 1 The total loss δ and the non-absorption background $\delta_0 - G_{\mathrm{EDFA}}$ in one sweep

3 Sensor design

3.1 Experimental configuration

Figure 2 schematically depicts the configuration of the wavelength-scanned all-fiber FLRDS system. A tunable DFB-LD (NLK1L5GAAA, NTT Electronics) with an emission of ~ 1572.5 nm is utilized as the light source. An optical switch (SWDR-11a261111, Agiltron Inc.) with a rising time of ~ 100 ns is used to inject optical pulses into an active fiber loop. The active fiber loop comprises coupler 1, an EDFA, a three-port fiber circulator, an FBG, a fiber delay line, coupler 2, a variable attenuator, and a fiber-integrated Herriot gas cell (3-m optical length). Coupler 1 and coupler 2 have a coupling ratio of 10:90 and 30:70, respectively. The EDFA, with a wide gain band (1570–1602 nm), is used to compensate for the cavity loss. The fiber delay line, having a length of 3 km, is necessarily inserted inside the cavity to separate two successive optical pulses in the time domain with an interval of ~ 15 μs. The FBG (grating length: 10 mm; reflectivity: > 90%; FWHM: 0.2 nm) filters the ASE noise from the EDFA before coupling out the fiber loop. An optical pulse starts to ring down in the cavity after applying a 5-μs-width electrical pulse on the optical switch. The ring-down signal is thereby detected by a fast photodetector (PDA20CS2, Thorlabs) and digitized by a low-noise data acquisition card (NI USB-6356, National Instruments). The ring-down time is then calculated after performing a fast simple exponential fitting.

3.2 Step-wise wavelength scanning

To identify the target absorption line, we perform a step-wise spectral scan by tuning the wavelength of the laser with a step of ~ 15 pm (this value is set as ~ 7 pm near the absorption peak). A custom-LabVIEW program with its flow chart shown in Fig. 3 is developed to carry out the working process of wavelength-scanned FLRDS. At the beginning, the wavelength of the seed laser is set to λ_0 (~ 1572.60 nm) and the 1f-lock process (detailed in the following paragraph) is performed to lock the fiber loop to the seed laser. Then, with a direct current voltage on the PZT, a light pulse is injected into the fiber loop for cavity ring down using the fast optical switch. After the FLRDS signal is completely recorded, the wavelength of the seed laser increases by $\Delta\lambda$. The 1f-lock process and cavity ring down are implemented in sequence. The above process reproduces until the whole absorption line is measured.

The FBG determines the fiber loop operation wavelength, its tunability is obtained by attaching the FBG to a PZT (SA050510, Piezodrive) sandwiched by a pair of lightweight aluminous blocks (shown in Fig. 2). With the PZT stretched, driven by a voltage amplifier (MDT694B, Thorlabs), the FBG center wavelength λ_B drifts by $\Delta\lambda_B$ as,

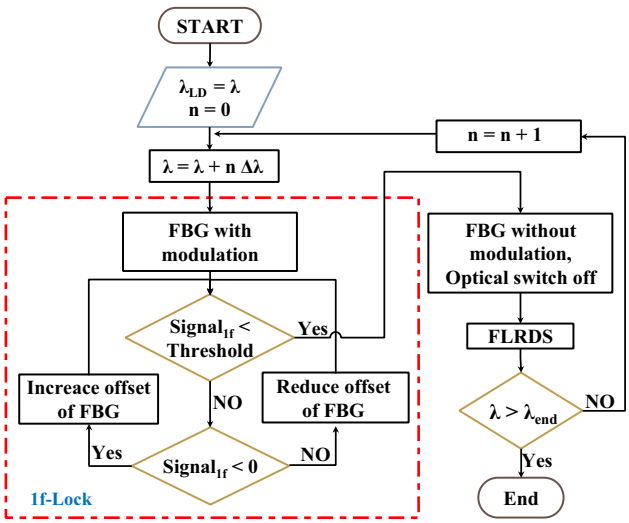

Fig. 3 Wavelength-scanned FLRDS flow chart using LabVIEW

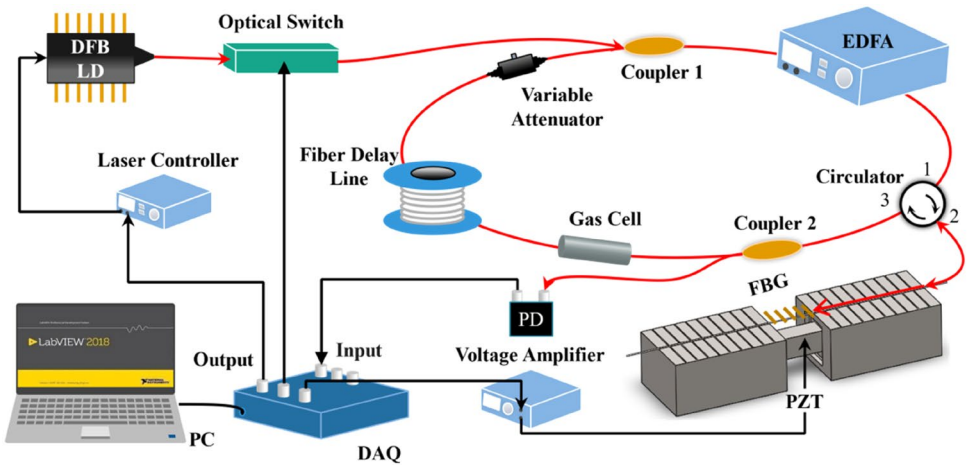

Fig. 2 Schematic of wavelength-scanned all-fiber FLRDS system. *DFB-LD* distributed feedback laser diode, *EDFA* erbium-doped fiber amplifier, *FBG* fiber Bragg grating, *PZT* piezoelectric transducer, *PD* photodetector, *DAQ* data acquisition card

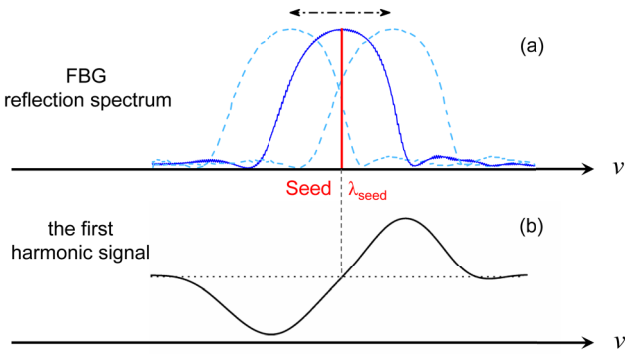

Fig. 4 **a** Reflection spectrum of the FBG and **b** the corresponding 1f signal with FBG sweeped and modulated across the seed laser wavelength

$$\frac{\Delta\lambda_B}{\lambda_B} = \left(1 - P_e\right) \cdot \kappa\,, \tag{7}$$

where P_e is the elastomeric coefficient and κ is the axial strain. To achieve a stable ring down, it is necessary to suppress the potential FBG wavelength drift from temperature fluctuation or mechanical vibration [21]. The FBG, having a reflection of a Gaussian-like profile as shown in Fig. 4a, enables one to achieve wavelength matching by performing an odd harmonic locking technique [18]. With a slow ramp and a fast sinusoidal modulation on the PZT (scanning frequency: 0.2 Hz; modulation frequency: 500 Hz; modulation depths: 10.5 V, corresponding to ~ 60 pm), the corresponding first harmonic (1f) signal is shown in Fig. 4b. Different from laser diodes [22, 23], negligible residual amplitude modulation exists in FBG-based wavelength modulation [24]. Thus, the symmetry point of the 1f signal at zero corresponds to the center wavelength of the FBG [25]. A LabVIEW subprogram of Proportion-Integration-Differentiation (PID) iteratively tunes the offset voltage on the PZT until the error signal, i.e., 1f value, closes to zero, indicating that the operation wavelength matches the laser wavelength. Here, the wavelength locking technique is called 1f-lock process.

4 Experimental results

We chose CO_2 as a spectroscopic target to demonstrate the wavelength-scanned FLRDS technique. After assembling the FBG-assisted filter, we used a wavemeter (771B-MIR, Bristol Instruments, accuracy: ± 1 ppm) to characterize its operation wavelength range by monitoring the FBG reflection of an ASE light source. By increasing the voltage on the PZT from 0 to 150 V, we obtained a 1-nm spectral range from 1572.5 to 1573.5 nm shown in the inset of Fig. 5, covering the overtone CO_2 absorption transitions of R(10), R(12), and R(14) in the L band. The

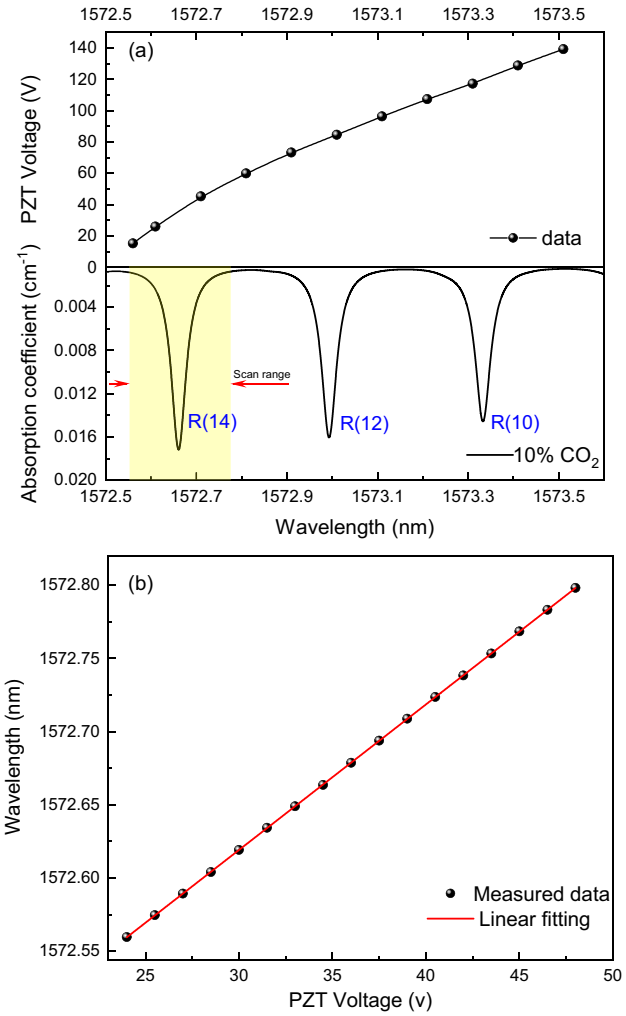

Fig. 5 **a** The spectral range with full driving voltage range, covering the overtone CO_2 absorption transitions of $R(10)$, $R(12)$, and $R(14)$ in the L band. **b** Center wavelength of the FBG-assisted fiber filter as a function of PZT voltage, a 250-pm spectral range with a good linear response is used to for the demonstration

slight nonlinear wavelength response to the PZT voltage is caused by the hysteresis of the PZT actuator [26]. In the implementation, we focused on a narrower spectral range of ~ 250 pm (1572.6–1572.85 nm) to cover the stronger CO_2 absorption transition at 6358.654 cm^{-1} [line intensity: 1.749×10^{-23} $cm^{-1}/(molec \cdot cm^{-2})$]. A good approximation of the linear fitting line to the calibrated wavelength points reveals a conversion factor of 10 pm/V. The calculated R^2 value is about 1. Thus, a linear wavelength modulation can be applied to the fiber loop by simply driving the PZT for both wavelength scanning and 1f-lock process.

With a light pulse injected into the fiber loop, dozens of decaying pulses were observed at the output of coupler 2 (shown in Fig. 2). One-hundred ring-down curves were measured and averaged to improve the SNR. Extracting the

maxima of these pulses, we performed an exponential fitting to the decaying tendency to figure out the 1/e ring-down time t_r as

$$y = y_0 + Ae^{-t/t_r} \tag{8}$$

After the records of the ring down for each wavelength, the LabVIEW-driven laser current was automatically increased by 2.5 mA to the next wavelength until the whole absorption profile was covered. The typical wavelength-scanned ring-down signal for pure CO_2 sample (0.8 atm, 296 K) is presented in Fig. 6. The measured black data correspond to the case when the laser wavelength is away from the absorption. In this case, no absorption exists even with the presence of the analyte, showing the inherent cavity loss. Similarly, the red and blue data and curves represent the cases when the laser wavelength is at approximate the half height of the absorption peak and the absorption line center, respectively. All the three coefficients of determination, i.e., calculated R-square values, are larger than 0.9995, indicating a good approximation of exponential fitting to the measured data.

The original measured results are shown in Fig. 7a. It is of interest to observe a slight slant added on the recovered spectrum. This influence derives from the non-flat gain curve of EDFA over wavelength which can be mitigated by employing an EDFA with automatic gain control, or by subtracting the direct wavelength-scanned FLRDS measurement of gain baseline, as a reference. We choose the latter method due to its low cost and simple implementation. In such a narrow spectral width compared with the whole L band, the gain baseline can be approximated by

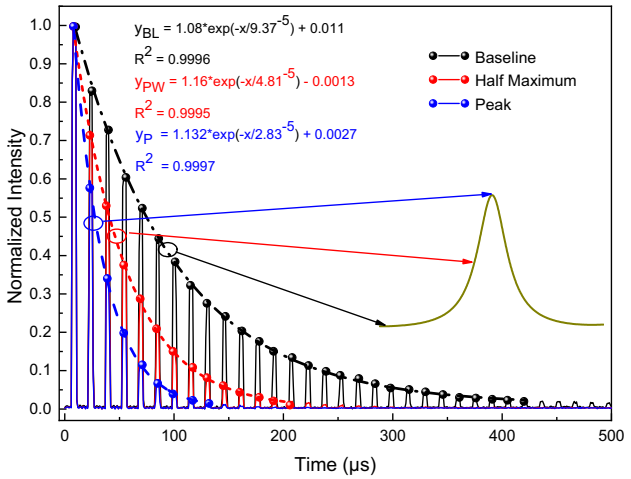

Fig. 6 Wavelength-scanned FLRDS signals for the CO_2 absorption spectrum around 6358.6 cm^{-1}. Typical ring-down curves for wavelengths away from the absorption line (Black), at approximate the half height of the absorption peak (Red) and at absorption line center (Blue)

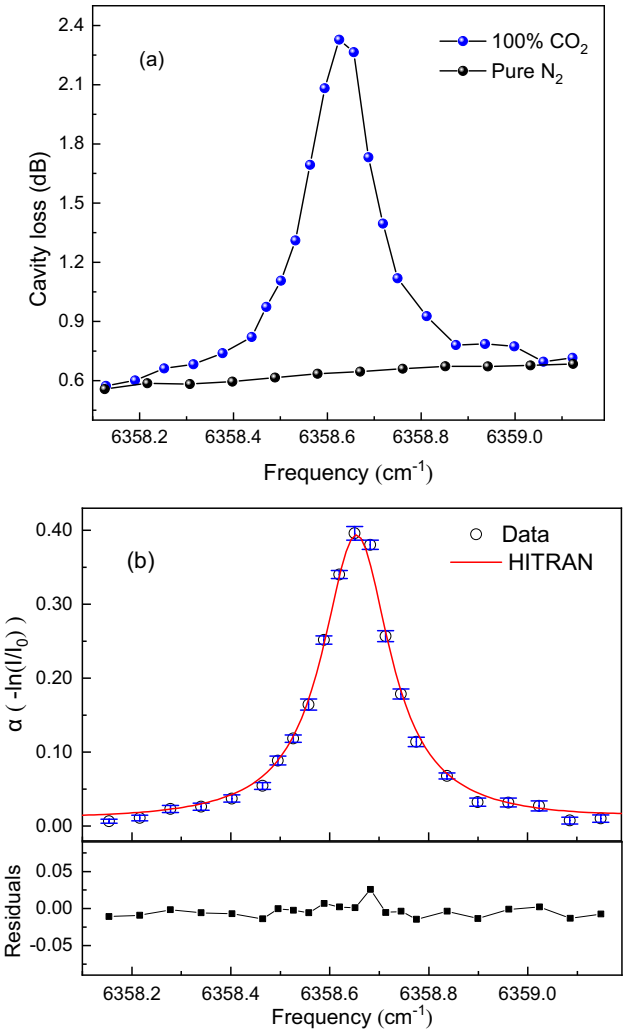

Fig. 7 **a** Measured raw data with pure CO_2 and pure N_2; **b** The comparison between the processed results and a profile computed using the HITRAN spectral paramters, Error bars show the standard deviation for ten measurements, the standard deviation of the residuals is 0.00862, at the noise level.

a linear fitting, which is confirmed by measurement with CO_2 emptied from the gas cell using pure N_2. After a prior calibration of gain baseline, the corrected absorption spectra in Fig. 7b can be well fitted by a profile computed using the HITRAN spectral parameters, showing an R-square value of 0.9964. With the absorption curve fitted, the gas concentration can be then obtained using Eq. (6) by calculating the integral area A.

We evaluated the system response by measuring CO_2 samples with different concentrations. Here the gas samples ranging from 10 to 100% were generated by diluting pure CO_2 with N_2 for the experimental test at 0.8 atm and 296 K. Figure 8 shows a direct comparison between the experimental results and theoretically calculated values using HITRAN spectral parameters of CO_2 transition of $R(14)$.

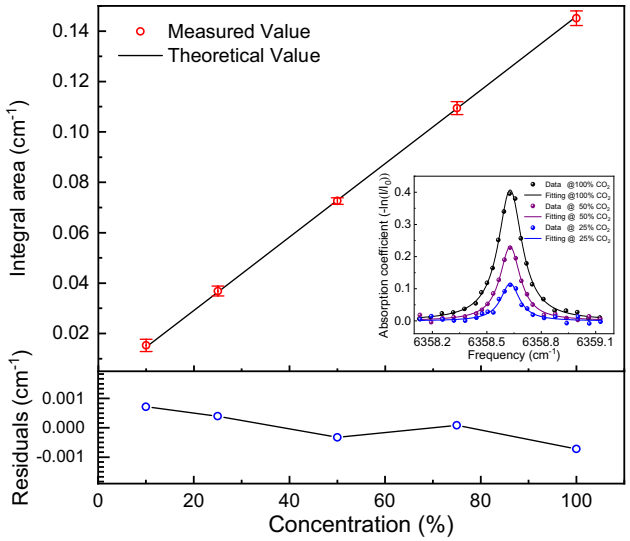

Fig. 8 The comparison between the theoretically calculated values and the experimental values. The residuals are plotted at the bottom panel, Error bars show the standard deviation for ten measurements. Inset: Typical processed data and fitting curves of different concentrations

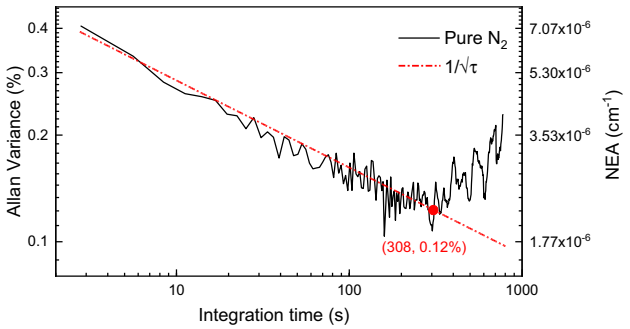

Fig. 9 Allan deviation analysis of the wavelength-scanned FLRDS sensor as a function of integration time. The measurement was carried out with gas cell filled with pure N_2

The maximum residual is only 0.00072 cm^{-1}, corresponding to a relative error of 0.28% for pure CO_2.

To evaluate the long-term stability of this sensor, an Allan deviation analysis was performed by measuring the cavity loss using pure N_2. Figure 9 shows the Allan deviation results. The data decrease inversely linearly with the square root of time, i.e., $\tau^{-1/2}$, when the white noise dominates the measurements. The minimum in the Allan deviation corresponds to the detection limit at the optimum integration time. It is observed that when the optimum integration time is 308 s, the minimum detection limit (MDL) of ~ 0.12% could be achieved, corresponding to a noise equivalent absorption (NEA) coefficient of 2.15×10^{-6} cm^{-1}. In addition, good system stability was proven according to the long optimum integration time over 300 s.

5 Discussion

The reported results reveal that the wavelength-scanned all-fiber FLRDS is capable of gas sensing in the L band with high sensitivity, fast response, and compact size. It is of interest to discuss the possible methods to enhance its versatility toward practical applications. An FBG-assisted optical filter was used in the demonstration experiments, which can only cover about 1-nm spectral range. It can be further to extended by employing a wider fiber Fabry–Perot tunable optical filter [27], or multiple FBGs in series [16]. Thus the measurement of multiple gases could be realized with the full advantages of the L band. Furthermore, the temperature could also be inferred by the ratio of two line strengths [28], with the extended working spectral range.

Considering the weak gas absorption in the L band, noise factors, such as ASE, temperature fluctuations and mechanical vibrations of the fiber loop, become the limitations on the current system sensitivity. Besides, for the active fiber loop used in this work, it is feasible to decrease its empty cavity loss by adjusting the attenuator or the optical gain G_{EDFA}. A higher sensitivity could be obtained as a lower empty cavity loss leads to a stronger laser-gas interaction and a longer ring-down time. However, we must consider a tradeoff between the sensitivity and the flat gain profile of the EDFA. Because the optical noise would be more serious when the gain is close to the threshold, i.e., empty loss equals zero. It could happen at the tail of the ring down as lower input power corresponds to a higher gain as shown in the gain curve of this current EDFA versus input power (see Appendix A). The improvements in the ASE noise using a narrower bandwidth filter, stability of EDFA gain with active gain control, as well as proper temperature or mechanical compensation should be focused on in future work.

6 Conclusion

We investigate an all-fiber wavelength-scanned CRDS technique for gas sensing in the L band. An active fiber loop is used to compensate for the cavity loss introduced by the fiber couplers, splices, and transmission. Besides, a LabVIEW-based automatic wavelength scanning process enables the simultaneous knowledge of the empty cavity loss as well as the whole absorption spectrum within the same scanning. This therefore can mitigate the complication of the frequent background recalibration and the risk of seed laser frequency drift. We further demonstrate this technique for CO_2 measurement. The recovered absorption

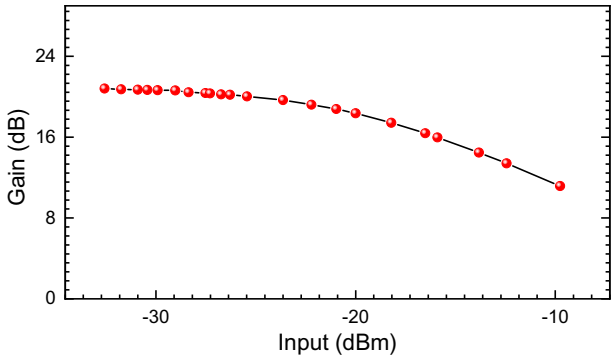

Fig. 10 Gain curve of the EDFA as a function of input power

spectrum matches the HITRAN-based theoretical simulation well with an R-square of 0.9964 and a minimum detection limit of 0.12% (corresponding to an NEA of 2.15×10^{-6} cm^{-1}) is achieved at 308-s integration time. Several strategies for further improving the system versatility are discussed. Hence, this investigation offers a technique to realize sample, sensitive, and long-term stable chemical analysis.

Appendix A: Gain curve characterization of the EDFA

The gain curve of the EDFA is calibrated. The seed laser is divided into two beams by a 50:50 coupler after a manually adjustable attenuator. With one branch connected to the EDFA, its input power is attenuated from 0.1 mW to 0.5 μW. The output power of EDFA is measured after being filtered by the FBG. The calibration result is shown in Fig. 10.

Acknowledgements This research was supported by Strategic Priority Research Program of Chinese Academy of Sciences (XDA17040513, XDA22020502), National Natural Science Foundation of China (62005267), Scientific Instrument Developing Project of the Chinese Academy of Sciences (YJKYYQ20190037), the Second Comprehensive Scientific Investigation of the Qinghai-Tibet Plateau (2019QZKK020802).

References

1. A. O'Keefe, D.A. Deacon, Rev. Sci. Instrum. **59**(12), 2544–2551 (1988)
2. P. Zalicki, R.N. Zare, J. Chem. Phys. **102**(7), 2708–2717 (1995)
3. G. Berden, R. Peeters, G. Meijer, Int. Rev. Phys. Chem. **19**(4), 565–607 (2000)
4. Y. Chen, K.K. Lehmann, J. Kessler, B.S. Lollar, G.L. Couloume, T.C. Onstott, Anal. Chem. **85**(23), 11250–11257 (2013)
5. W. Yuan, D. Zheng, J. Jiang, Y. Chao, IEEE Trans. Instrum. Meas. (2021).
6. L.S. Rothman, I.E. Gordon, Y. Babikov, A. Barbe, D.C. Benner, P.F. Bernath, M. Birk, L. Bizzocchi, V. Boudon, L.R. Brown, J. Quant. Spectrosc. Radiat. Transfer **130**, 4–50 (2013)
7. G. Stewart, K. Atherton, H. Yu, B. Culshaw, Meas. Sci. Technol. **12**(7), 843 (2001)
8. D.E. Vogler, M.G. Müller, M.W. Sigrist, Appl. Opt. **42**(27), 5413–5417 (2003)
9. G. Stewart, K. Atherton, B. Culshaw, Opt. Lett. **29**(5), 442–444 (2004)
10. N. Ni, C. Chan, T. Chuah, L. Xia, P. Shum, Meas Sci Technol **19**(11), 115203 (2008)
11. Y. Zhao, L. Bai, Q. Wang, Opt Commun **309**, 328–332 (2013)
12. C. Zhu, G. Wang, Z. Zheng, R. Wang, X. Tao, P. Wang, IEEE Photonics J. **8**(5), 1–8 (2016)
13. Y. Wang, G.-M. Ma, D. Zheng, W.-Q. Qin, J. Jiang, H.-Y. Zhou, C. Yan, Sens Actuators B Chem **346**, 130590 (2021)
14. Y. Zhao, L. Bai, B. Han, Q. Wang, Instrum Sci. Technol. **41**(4), 349–364 (2013)
15. S.O. Silva, R. Magalhães, M. Marques, O. Frazão, Opt. Laser Technol. **78**, 115–119 (2016)
16. Y. Zhao, J. Chang, J. Ni, Q. Wang, T. Liu, C. Wang, P. Wang, G. Lv, G. Peng, Opt. Express **22**(9), 11244–11253 (2014)
17. R. S. Vodhanel, M. Krain, R. E. Wagner, W. B. Sessa, Opt. Soc. Am. WG5 (1994).
18. Q. Wang, Z. Wang, W. Ren, Meas Sci Technol **28**(6), 065102 (2017)
19. T. Von Lerber, M.W. Sigrist, Appl. Opt. **41**(18), 3567–3575 (2002)
20. M. Lackner, Rev. Chem. Eng. **23**(2), 65–147 (2007)
21. J. Nedoma, M. Fajkus, L. Bednarek, J. Frnda, J. Zavadil, V. Vasinek, Adv. Electr. Electr. Eng. **14**(4), 460–466 (2016)
22. K. Sun, X. Chao, R. Sur, C. Goldenstein, J. Jeffries, R. Hanson, Meas, Sci. Technol. **24**(12), 125203 (2013)
23. Q. Wang, J. Chang, W. Wei, C. Zhu, C. Tian, Appl. Phys. B **117**(4), 1015–1023 (2014)
24. Q. Wang, Z. Wang, W. Ren, P. Patimisco, A. Sampaolo, V. Spagnolo, Sens. Actuators B Chem. **268**, 512–518 (2018)
25. H. Li, G.B. Rieker, X. Liu, J.B. Jeffries, R.K. Hanson, Appl. Opt. **45**(5), 1052–1061 (2006)
26. K. Liu, W. Jing, G. Peng, J. Zhang, D. Jia, H. Zhang, Y. Zhang, Opt. Commun. **281**(12), 3286–3290 (2008)
27. L. Yu, T. Liu, K. Liu, J. Jiang, L. Zhang, Y. Jia, T. Wang, Sens. Actuators B Chem. **193**, 356–362 (2014)
28. X. Zhou, J. Jeffries, R. Hanson, Appl. Phys. B **81**(5), 711–722 (2005)